Research Article

Kalachar Karthik, Rania Saadeh, Ravikumar Shashikala Varun Kumar, Ahmad Qazza, Javali Kotresh Madhukesh, Umair Khan*, Anuar Ishak, and Md Irfanul Haque Siddiqui

Computational analysis of water-based silver, copper, and alumina hybrid nanoparticles over a stretchable sheet embedded in a porous medium with thermophoretic particle deposition effects

https://doi.org/10.1515/ntrev-2024-0083
received January 20, 2024; accepted July 24, 2024

Abstract: The present study scrutinizes the significance of heat source/sink (HSS), thermophoretic particle deposition, and porous media on the time-dependent ternary nanofluid stream across a stretchable surface in the presence of Newtonian heating (NH) and common wall temperature (CWT) cases. The governing equations of the investigated model are changed into ordinary differential equations by using suitable similarity transformations. The resultant dimensionless equations are solved using the Laguerre polynomial collocation method. For comparison, the Runge Kutta Fehlberg's fourth-fifth order (RKF-45) method is employed. Graphs are used to illustrate the significant parameters' impacts on each profile, and relevant physical quantities such as the Sherwood number, skin friction, and Nusselt number are exhibited. The study reveals that the velocity profile drops with an increase in permeable parameters. The thermal profile increases with improvement in porous and HSS constraints. The concentration diminishes as the value of the thermophoretic parameter rises. For better solid volume fraction values, the rate of temperature dispersal is lower in the NH case associated with the CWT case. Additionally, the rate of thermal distribution is enhanced by approximately 2.90% surface drag force, 4.73% in the CWT case and 2.27% in the NH case, and the rate of mass transfer is enhanced by 2.99% when transitioning from ternary the ternary hybrid nanofluid to the (normal) nanofluid. The results of the study will help in heat exchangers, thermal management, chemical engineering, biomedical instruments, and design and optimization of electronic equipment.

Keywords: ternary hybrid nanofluid, heat source/sink, thermophoretic particle deposition

*** Corresponding author: Umair Khan,** Department of Mathematical Sciences, Faculty of Science and Technology, Universiti Kebangsaan Malaysia, UKM, Bangi 43600, Selangor, Malaysia; Department of Mathematics, Faculty of Science, Sakarya University, Serdivan/Sakarya 54050, Turkey; Department of Computer Science and Mathematics, Lebanese American University, Byblos, Lebanon; Department of Mechanics and Mathematics, Western Caspian University, Baku 1001, Azerbaijan, e-mail: umairkhan@sakarya.edu.tr, umair.khan@lau.edu.lb
Kalachar Karthik: Department of Studies in Mathematics, Davangere University, Davangere 577002, India, e-mail: karthikkalachar@gmail.com
Rania Saadeh: Faculty of Science, Zarqa University, Zarqa 13110, Jordan, e-mail: rsaadeh@zu.edu.jo
Ravikumar Shashikala Varun Kumar: Department of Pure and Applied Mathematics, School of Mathematical Sciences, Sunway University, Petaling Jaya 47500, Selangor Darul Ehsan, Malaysia, e-mail: varursv@gmail.com
Ahmad Qazza: Faculty of Science, Zarqa University, Zarqa 13110, Jordan, e-mail: aqazza@zu.edu.jo
Javali Kotresh Madhukesh: Department of Mathematics, GM University, Davangere, 577006, India, e-mail: madhukeshjk@gmail.com
Anuar Ishak: Department of Mathematical Sciences, Faculty of Science and Technology, Universiti Kebangsaan Malaysia, UKM, Bangi 43600, Selangor, Malaysia, e-mail: anuar_mi@ukm.edu.my
Md Irfanul Haque Siddiqui: Mechanical Engineering Department, College of Engineering, King Saud University, Riyadh 11451, Saudi Arabia, e-mail: msiddiqui2.c@ksu.edu.sa

Nomenclature

C_1	concentration
ρ	density (kg m^{-3})
D_B	diffusivity (m^2 s^{-1})
(x, y)	directions (m)
μ	dynamic viscosity (kg m^{-1} s^{-1})
q_w	heat flux
Q_0	heat source/sink (W m^{-3} K^{-1})
Hs	heat source/sink parameter
h_s	heat transfer parameter
ν	kinematic viscosity (m^2 s^{-1})
J_w	mass flux

Open Access. © 2024 the author(s), published by De Gruyter. This work is licensed under the Creative Commons Attribution 4.0 International License.

Δ	Newtonian heating parameter
Nu_x	Nusselt number
K^*	porosity (m^2)
λ	porous parameter
Pr	Prandtl number
T_r	reference temperature
Re	Reynolds number
Sc	Schmidt number
τ_w	shear stress
Sh_x	Sherwood number
Cf_x	skin friction
ϕ	solid volume fraction
C_p	specific heat ($J\ kg^{-1}\ K^{-1}$)
a	stretching rate (s^{-1})
u_w	stretching velocity ($m\ s^{-1}$)
T_1	temperature (K)
k	thermal conductivity ($kg\ ms^{-3}\ K^{-1}$)
α	thermal diffusivity ($m^2\ s^{-1}$)
τ_1	thermophoretic parameter
V_T	thermophoretic velocity
t	time (s)
γ_1	unsteadiness parameter
(u_1, v_1)	velocity components ($m\ s^{-1}$)

Subscript

thnf	ternary hybrid nanofluid
nf	nanofluid
f	fluid
hnf	hybrid nanofluid
w	wall
∞	ambient

Abbreviations

BC	boundary condition
BVP	boundary value problem
CWT	common wall temperature
HSS	heat source/sink
LPCM	Laguerre polynomial collocation method
NH	Newtonian heating
ODE	ordinary differential equation
RKF-45	Runge Kutta Fehlberg's fourth-fifth-order method
T-HNF	ternary hybrid nanofluid
TPD	thermophoretic particle deposition

1 Introduction

The development of metal particles has led to the creation of a new class of fluid recognized as nanofluids, which are made of tiny materials with a diameter of just a few nanometers. A two-phase mixture is created when very small metallic particles, or nanomaterials, are combined with a saturated liquid. The temperature conductivity of these liquids is far more important than that of the basic liquid. It has been discovered that nanofluids offer greater thermal and physical attributes to basic liquids. Under the conditions of the creation of various kinds of innovation based on nanotechnology, a new liquid for heat removal was produced, which led to technical innovation worldwide. There are hybrid nanofluids with enhanced thermal conductivity. Ternary hybrid nanofluids (T-HNFs) are the most recent finding. Even two forms of nanoparticles tightly incorporated into the base liquid offer better possibilities in terms of heat transmission and total efficacy. Albalawi *et al.* [1] investigated the thermal distribution of nanofluid and its aggregation impacts over a coaxial cylinder. Kumar *et al.* [2] explored the ternary nanofluid movement in the presence of magnetic dipole over forced, mixed, and free convection scenarios. Vinutha *et al.* [3] examined the MHD ternary nanofluid stream among two parallel plates with RSM and sensitivity analysis. With the impact of entropy production, Salawu *et al.* [4] explored the thermal power application of the nanofluid stream through a vertical channel. The flow of nanoliquid past a stretchy plate with the consequence of thermal radiation was probed by Oke *et al.* [5]. Madhu *et al.* [6] looked into the heat transport analysis of the nanofluid stream through a revolving cone. Wang *et al.* [7] probed the influence of the flow of nanofluid across the stretchable surface with heat and mass transport attributes. The stream of ternary nanofluid past a stretching surface with the effect of an entropy generation was scrutinized by Khan *et al.* [8]. Karthik *et al.* [9] delineated the flow of ternary nanofluid past a wedge with a radiation impact. Saadeh *et al.* [10] conducted a study on statistical analysis for computing two-point fuzzy boundary value issues by replicating the kernel scheme.

Nanoparticles like silver, copper, and alumina have diverse applications in real life. First, silver nanoparticles play a prominent role in the medical field, which includes dressings for injuries, surgical implants, and delivery of drug devices. Several authors investigated the synthesis and applications of silver nanoparticles. According to Marin *et al.* [11], silver nanoparticles have a constant quantity of flexible qualities, which supports a wider range of uses in biomedical and related domains. Beyene *et al.* [12] conducted a review of

the manufacturing paradigm and uses of silver nanoparticles. Abou El-Nour *et al.* [13] looked into the synthesis of silver nanoparticles as well as their uses. Second, copper nanoparticles are well acknowledged because of their exceptional ability to conduct heat and electricity. These features render them essential in the electronics sector, where they are employed in interconnects, printed circuit panels, and as fillers with conductivity in sealants and varnishes. Copper nanoparticles are also being investigated for their applications in antibacterial paints, farming, and as additives in lubrication and polymers. Din and Rehan [14] investigated the possibility of fabricating copper nanoparticles with a variety of structural features and beneficial biological effects by using novel environmentally friendly techniques. According to Crisan *et al.*'s [15] study, one of the elements that are most prevalent and essential to an organism's regular operation is copper. Kumar *et al.* [16] investigated a polyethyleneimine–chromium oxide compound sensor with a perforated copper clad as its substrate for sensing. Further, alumina nanoparticles, which are made of aluminum oxide, possess remarkable hardness, exceptional thermal resistance, and chemical insensitivity. These characteristics render them highly beneficial for the manufacturing of stones, pottery, and refractory components utilized in the creation of cutting instruments, polishing axles, and other products requiring high temperatures. Alumina nanoparticles are utilized as catalyst supports in the discipline of catalysis because of their expansive surface area and temperature durability, which enable a wide range of chemical reactions and treatment of environmental-related issues. Ziva *et al.* [17] assessed recent advancements in the manufacturing of aluminum oxide nanoparticles. There are several industrial uses for alumina. Omodele *et al.* [18] looked at the usage of aluminum as an early stage for the creation of nanoparticles for water purification. Pourmadadi *et al.* [19] investigated the production and properties of porous alumina to create feasible nanotechnology for drug delivery applications. Mahesh *et al.* [20] evaluated the removal of contaminants from groundwater using alumina-based nanoparticles.

It has already become a crucial word of concept in the 22nd century of engineering due to its wide impact on numerous branches of this vast field. Permeable media (a system of holes or pores interconnected in a solid matrix) has aroused great interest within mechanics-framework for liquids. As we look at more complex engineering problems, such as liquid flow in living tissues, groundwater movement, and storage of the oil reserves that may not be visible to others outside this industry but affect our very lives, porous medium research and application are becoming increasingly important. Alhadhrami *et al.* [21] investigated the chemical reactions' impact on the stream of fluid past a stretchy surface. Shamshuddin *et al.* [22] scrutinized the stream of fluid across a permeable medium with the influence of convection. Wang *et al.* [23] explored the flow of nanoliquid *via* a stretchy surface in a porous media. The consequence of the magnetic effect on the liquid stream in a porous stretchable surface was estimated by Alhadhrami *et al.* [24]. Dharmendar Reddy *et al.* [25] scrutinized the stream of heat transfer liquid through the stretchy sheet immersed in a permeable medium. While analyzing a situation in which there are significant temperature variations between the liquid at the surface and the environmental liquid, the term "heat source/sink (HSS)" is employed in the study of thermal energy. Because there are so many different ways that heat sources and sinks are used in energy preservation methods, scientists must investigate ways to control their characteristics in engineering difficulties to meet contemporary needs. Wang *et al.* [26] delineated the stream of liquid past the stretchy shallow with the consequence of HSS. The impact of HSS on the Rabinowitsch liquid stream *via* a circular tube was delineated by Chu *et al.* [27]. The flow of nanoliquid across an elongated surface in the presence of HSS was inspected by Thumma *et al.* [28]. The fractional diffusion equation numerical solutions employing a finite-difference approach were studied by Saadeh [29]. The stream of magnetized micropolar liquid *via* a porous stretched sheet with an HSS was debriefed by Ram *et al.* [30].

In many engineering processes, such as heat exchangers, air cleaners, building ventilation systems, nuclear reactor safety, and powdered coal burners, thermophoretic particle deposition (TPD) in the flow of liquid is crucial. The thermophoresis phenomenon is the consequence of different particle kinds responding differently to a temperature gradient. Thermophoresis is a process that dramatically raises the depositing motion of minute particles in the way of decreasing temperature but has no effect on huge particles. Small, minute nanoparticles deposited in a nonisothermal gas will develop a velocity in this process. Thermophoresis is the process by which minute particles settle on a cold surface. Wang *et al.* [31] inspected the significance of TPD on the fluid movement *via* an inclined surface. Bai *et al.* [32] conducted a study on the theoretical computation of the environmental and economic advantages of dam flow using open-source field operations and modification. By using the heat flux model, Bashir *et al.* [33] probed the flow of liquid through a stretchable surface with the TPD effect. The stream of the Oldroyd-B fluid across the stretchy sheet with the upshot of radiation and TPD was elongated by Wang *et al.* [34]. The flow of liquid *via* a cylinder with the consequence of TPD was examined by Yasir *et al.* [35]. Many researchers were interested in the influence of the fluid flow field on stretching sheets, leading

to a large amount of study being done. Shaping is one of the most significant industrial operations that has historically been used to increase ductility and high-precision part manufacture. Numerous technical problems can be solved by studying the fluid flow on stretched sheets, including casting, drawing or plastic films, hot rolling, polymer extrusion, and others. Shamshuddin *et al.* [36] deliberated the stream of liquid *via* a stretchy sheet with the magnetic impact. Alsaiari *et al.* [37] conducted computational research on heat transfer and circulation resistance in a solar-powered air conditioner with a ribbed absorption panel. Saadeh *et al.* [38] conducted a case study on the mathematical simulation and stability analysis of the innovative fraction model in the derivative of the Caputo operator. Shamshuddin *et al.* [39] investigated the flow of nanoliquid across a stretchable surface using a quasi-linearization approach. Utilizing homotopic simulation, Shamshuddin *et al.* [40] probed the motion of nanofluid across a stretchy sheet.

The influences of HSS, TPD, and porous media are examined concerning the time-dependent T-HNF stream across a stretchy surface. Further, Newtonian heating (NH) and common wall temperature (CWT) scenarios are considered for inspecting the heat transfer analysis in the present investigation. Suitable similarity transformations are used to convert the governing equations of the studied model into ordinary differential equations (ODEs). By using Laguerre polynomial collocation method (LPCM), the resulting dimensionless equations are solved and the RKF-45 is employed for the comparison of the achieved numerical results. The influence of various factors on the different profiles is exhibited with the aid of graphical representations.

The following research questions are the focus of the present work's investigation.

(1) What are the changes observed in the velocity profiles for changing values of porous parameters?
(2) How does the HSS parameter affect the temperature profile with CWT and NH case?
(3) How will the thermophoretic parameter impact the concentration profile?

2 Mathematical background of the problem

Let's examine an incompressible, time-dependent, two-dimensional T-HNF flow with the consequence of HSS and TPD across a stretched surface. Let (u_1, v_1) be the velocity in the (x, y) direction as depicted in Figure 1. The temperature and concentration are taken as T_1 and C_1.

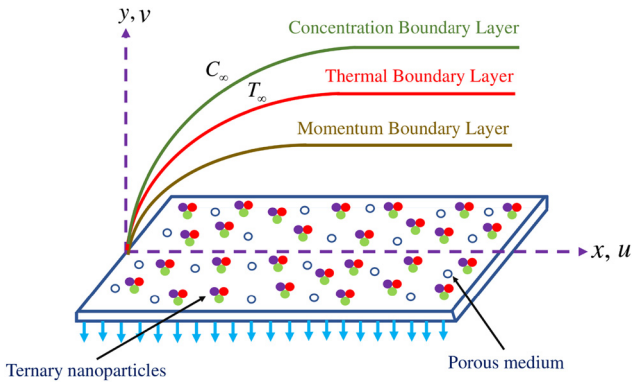

Figure 1: Design of the flow problem.

The ambient temperature and far-field concentration are assumed as T_∞ and C_∞. Wall concentration is denoted by C_w, and wall temperature is represented by T_w.

The stretchable velocity is given as $u_w = \frac{a\,x}{(1-\beta t)}$, $Q_0 = \frac{Q_1}{(1-\beta t)}$ is the rate of heat generation/absorption, and the porous medium permeability is indicated as $K^* = \frac{K_1}{(1-\beta t)^{-1}}$. On the basis of the aforementioned assumptions, the governing equations are given as follows [41–44]:

$$\frac{\partial u_1}{\partial x} + \frac{\partial v_1}{\partial y} = 0, \tag{1}$$

$$\frac{\partial u_1}{\partial t} + u_1\frac{\partial u_1}{\partial x} + v_1\frac{\partial u_1}{\partial y} = \nu_{\text{thnf}}\frac{\partial^2 u_1}{\partial y^2} - \frac{\nu_{\text{thnf}}}{K^*}u_1, \tag{2}$$

$$\frac{\partial T_1}{\partial t} + u_1\frac{\partial T_1}{\partial x} + v_1\frac{\partial T_1}{\partial y} = \alpha_{\text{thnf}}\frac{\partial^2 T_1}{\partial y^2} + \frac{Q_0}{(\rho C_p)_{\text{thnf}}}(T_1 - T_\infty), \tag{3}$$

$$\frac{\partial C_1}{\partial t} + u_1\frac{\partial C_1}{\partial x} + v_1\frac{\partial C_1}{\partial y} = D_B\frac{\partial^2 C_1}{\partial y^2} - \frac{\partial}{\partial y}(V_T(C_1 - C_\infty)). \tag{4}$$

Boundary conditions (BCs) [44]:

$$\begin{aligned} &u_1 = u_w,\ \ v_1 = 0,\ \ (\text{CWT} - \text{case})T_1 = T_w,\\ &(\text{NH} - \text{case})\frac{\partial T_1}{\partial y} = -h_s T_1,\ \ C_1 = C_w \ \text{ at } y = 0, \end{aligned} \tag{5}$$

$$u_1 \to 0,\ \ T_1 \to T_\infty,\ \ C_1 \to C_\infty \ \text{ as } y \to \infty. \tag{6}$$

The subsequent similarity variables are presented as follows:

$$\begin{aligned} \eta = y\sqrt{\frac{a}{\nu_f(1-\beta t)}},\ \ u_1 = \frac{ax}{(1-\beta t)}f',\ \ v_1 \\ = -\sqrt{\frac{a\nu_f}{(1-\beta t)}}f, \end{aligned} \tag{7}$$

$$\chi = \frac{C_1 - C_\infty}{C_w - C_\infty},\ \ \theta = \frac{T_1 - T_\infty}{T_w - T_\infty}(\text{CWT}),\ \ \theta = \frac{T_1 - T_\infty}{T_\infty}(\text{NH}). \tag{8}$$

2.1 TPD

It is assumed that the species concentration is low and that the species velocity in relation to external body forces is minimal. By using the boundary layer approach, Talbot *et al.* [45] provided the thermophoretic velocity. The thermophoretic velocity V_T is specified as follows:

$$V_T = -\nu_{thnf}\frac{\kappa}{T_r}\frac{\partial T_1}{\partial y}, \tag{9}$$

where T_r is the reference temperature, $\kappa\ \nu$ is the thermophoretic diffusivity, and κ is the thermophoretic coefficient. The values of κ will range from 0.2 to 1.2, as stated by Batchelor and Shen [46]. The most crucial element in figuring out the thermophoretic coefficient κ is the Knudsen number (Kn). There are several ways to evaluate κ depending on the flow regime in studies, and Talbot *et al.* [45] presents a clear definition of κ as follows:

$$\kappa = \frac{2C_s\left(\frac{\lambda_g}{\lambda_p} + C_t\mathrm{Kn}\right)\left(\mathrm{Kn}\left(C_1 + C_2e^{-\frac{C_3}{\mathrm{Kn}}}\right) + 1\right)}{(1 + 3C_m\mathrm{Kn})\left(1 + \frac{\lambda_g}{\lambda_p} + 2C_t\mathrm{Kn}\right)},$$

where λ_p and λ_g are the thermal conductivities of liquid and diffused particles, respectively. The constants is given by $C_1 = 1.2$, $C_2 = 0.41$, $C_3 = 0.8$, $C_s = 1.147$, $C_m = 1.146$, and $C_t = 2.20$.

The thermophoretic diffusion coefficient κ strongly depends on the Knudsen number, which is defined as the ratio of the gas mean free path l to the radius of the particle, and on the ratio of the gas and the particle thermal conductivities λ_g/λ_p. There are already a variety of equations available for calculating the thermophoretic diffusion coefficient κ, and they have been verified by experiments conducted for both low and high Knudsen numbers. For monoatomic gases, the formulas κ rely on the ratio of the gas to particle thermal conductivities (λ_g/λ_p) and are a function of the Knudsen number. However, it should be mentioned that translational conductivity is often used to determine the ratio of the gas and particle thermal conductivities in the case of polyatomic gases [45,47–49].

2.2 Conversion of governing equations and thermophysical properties

By substituting equations (7) and (8) into equations (2)–(4), we obtain the following reduced form:

$$\frac{f'''}{A_1A_2} - (f')^2 + ff'' + \gamma_1\left(\frac{\eta}{2}f'' - f'\right) - \frac{\lambda}{A_1A_2}f' = 0, \tag{10}$$

$$\frac{k_{thnf}}{k_f}\frac{\theta''}{\mathrm{Pr}} + A_3\left(\theta' f - \gamma_1\frac{\eta}{2}\theta'\right) + \mathrm{Hs}\,\theta = 0, \tag{11}$$

$$\frac{\chi''}{\mathrm{Sc}} + \chi' f - \gamma_1\frac{\eta}{2}\chi' - \frac{\tau_1}{A_1A_2}(\theta'\chi' + \chi\theta'') = 0, \tag{12}$$

and reduced BCs are

$$\begin{aligned} &f'(0) = 1,\ f(0) = 0,\ \theta(0) = 1(\mathrm{CWT}),\ \chi(0) = 1 \\ &\theta'(0) = -\Delta[1 + \theta(0)](\mathrm{NH})\ \text{at}\ \eta = 0, \end{aligned} \tag{13}$$

$$f'(\infty) = 0,\ \theta(\infty) = 0,\ \chi(\infty) = 0\ \text{as}\ \eta \to \infty, \tag{14}$$

where $\gamma_1 = \frac{\beta}{a}$ is the unsteadiness constraint, $\mathrm{Pr} = \frac{\nu_f(\rho C_p)_f}{k_f}$ signifies the Prandtl number, $\mathrm{Sc} = \frac{\nu_f}{D_B}$ is the Schmidt number, $\tau_1 = -\frac{\kappa(T_w - T_\infty)}{T_r}$ signifies the thermophoretic constraint, $\mathrm{Hs} = \frac{Q_1}{a(\rho C_p)_f}$ signifies the HSS constraint, $\lambda = \frac{\nu_f}{K_1 a}$ is the porous parameter, and $\Delta = h_s\sqrt{\frac{\nu_f(1-\beta t)}{a}}$ is the NH parameter. Moreover, the thermophysical properties are represented by the other symbols as follows:

$$A_1 = (1 - (\phi_1 + \phi_2 + \phi_3))^{2.5},$$

$$A_2 = \phi_3\left(\frac{\rho_{S3}}{\rho_f}\right) + \phi_2\left(\frac{\rho_{S2}}{\rho_f}\right) + \phi_1\left(\frac{\rho_{S1}}{\rho_f}\right) + (1 - \phi_1 - \phi_2 - \phi_3),$$

$$A_3 = \phi_3\left(\frac{\rho_{S3}C_{p3}}{\rho_f C_{pf}}\right) + \phi_2\left(\frac{\rho_{S2}C_{p2}}{\rho_f C_{pf}}\right) + \phi_1\left(\frac{\rho_{S1}C_{p1}}{\rho_f C_{pf}}\right) + (1 - \phi_3 - \phi_2 - \phi_1).$$

The thermophysical properties of T-HNF are given [50] in the following form:

$$\frac{\mu_{thnf}}{\mu_f} = \frac{1}{(1 - (\phi_3 + \phi_2 + \phi_1))^{2.5}},$$

$$\rho_{thnf} = (1 - (\phi_3 + \phi_2 + \phi_1))\rho_f + \phi_3\rho_{S3} + \phi_1\rho_{S1} + \phi_2\rho_{S2},$$

$$(\rho C_p)_{thnf} = (1 - (\phi_1 + \phi_2 + \phi_3))(\rho C_p)_f + \phi_2(\rho C_p)_{S2} + \phi_3(\rho C_p)_{S3} + \phi_1(\rho C_p)_{S1},$$

$$\frac{k_{thnf}}{k_{bf}} = \frac{\phi_2k_2 + \phi_3k_3 + \phi_1k_1 + 2(\phi_3 + \phi_2 + \phi_1)k_f + 2(\phi_3 + \phi_2 + \phi_1)(\phi_1k_1 + \phi_3k_3 + \phi_2k_2) - 2(\phi_3 + \phi_2 + \phi_1)^2k_f}{\phi_2k_2 + \phi_1k_1 + \phi_3k_3 + 2(\phi_3 + \phi_2 + \phi_1)k_f - (\phi_3 + \phi_2 + \phi_1)(\phi_1k_1 + \phi_2k_2 + \phi_3k_3) + (\phi_3 + \phi_2 + \phi_1)^2k_f}.$$

Here, ϕ is the solid volume fraction, ρ is density, μ is dynamic viscosity, C_p is heat capacity, and k is thermal conductivity. In the aforementioned expression, it will reduce for hybrid nanofluid for $\phi_3 = 0$ and it will also reduce to nanofluid expression when $\phi_3 = \phi_2 = 0$.

2.3 Gradients

The engineering physical quantities of interest are the skin friction coefficient, Cf_x, the heat transfer rate, Nu_x, and the mass transfer rate, Sh_x which defined as follows [51]:

$$\mathrm{Nu}_x = \frac{xq_w}{k_f(T_w - T_\infty)}, \quad \mathrm{Cf}_x = \frac{\tau_w}{\rho u_w^2} \text{ and } \mathrm{Sh}_x = \frac{xJ_w}{D_B(C_w - C_\infty)}. \tag{15}$$

The shear stress along the sheet is taken as $\tau_w = \mu_{thnf}\frac{\partial u_1}{\partial y}\Big|_{y=0}$, the heat flux from the sheet is given as $q_w = -k_{thnf}\frac{\partial T_1}{\partial y}\Big|_{y=0}$, and the mass flux from the sheet is depicted as $J_w = -D_B\frac{\partial C_1}{\partial y}\Big|_{y=o}$.

By using the similarity variables into the aforementioned expressions, we obtain

$$-\frac{k_{thnf}}{k_f}\theta'(0) = \frac{\mathrm{Nu}_x}{\sqrt{\mathrm{Re}}}, \quad A_1\mathrm{Cf}_x\sqrt{\mathrm{Re}} = f''(0), \text{ and } \frac{\mathrm{Sh}_x}{\sqrt{\mathrm{Re}}} = -\chi'(0). \tag{16}$$

The local Reynolds number is $\mathrm{Re} = \frac{u_w x}{\nu_f}$.

3 Elucidation of LPCM

The following expression is appropriate to develop Laguerre polynomials:

$$L_j(\zeta) = \frac{1}{j!}\left(\frac{d}{d\zeta} - 1\right)^j \zeta^j. \tag{17}$$

In addition, the aforementioned equation satisfies the recursive correlation as shown by

$$(j+1)L_{j+1}(\zeta) = (2n + 1 - \zeta)L_j(\zeta) - nL_{j-1}(\zeta), \tag{18}$$

$$\zeta L_j'(\zeta) = jL_\xi(\zeta) - jL_{j-1}(\zeta). \tag{19}$$

The first two terms $L_0(\zeta)$ and $L_1(\zeta)$ are obtained by using equation (15), and the subsequent terms can be determined by applying equations (18) and (19). The initial five terms, which are polynomials of different degrees, are given as follows:

$$\left.\begin{aligned} L_0 &= 1, \\ L_1 &= 1 - \zeta, \\ L_2 &= 1 - 2\zeta + \frac{1}{2}\zeta^2, \\ L_3 &= 1 - 3\zeta + \frac{3}{2}\zeta^2 - \frac{1}{6}\zeta^3, \\ L_4 &= 1 - 4\zeta + 3\zeta^2 - \frac{2}{3}\zeta^3 + \frac{1}{24}\zeta^4. \end{aligned}\right\} \tag{20}$$

The boundary value problem (BVP) of order n can be approximated by a linear combination of the Laguerre polynomials given in equation (20) as follows:

$$y(\zeta) = \sum_{j=0}^{N} a_j L_j(\zeta), \tag{21}$$

where $a_0, a_1, \ldots, a_N$ are constants to be determined. On differentiating the aforementioned equation up to n number of times and approximating the nth order BVP yields:

$$p_n(\zeta)\sum_{j=0}^{(N)} a_j L_j^{(n)}(\zeta) + p_{n-1}(\zeta)\sum_{j=0}^{N} a_j L_j^{(n-1)}(\zeta) + \cdots + p_1(\zeta)\sum_{j=0}^{N} a_j L_j'(\zeta) + p_0(\zeta)\sum_{j=0}^{N} a_j L_j(\zeta) = M(\zeta). \tag{22}$$

Like coefficients of equation (22) (a_j, $j = 0, 1, \ldots, N$) are accumulated after each term in equation (22) has been expanded, leading to:

$$\sum_{j=0}^{N} a_j(p_j^*(\zeta)Q(\zeta)) = M(\zeta). \tag{23}$$

Given that there is the same number of BCs and order of BVP in this study, with the help of the BCs, l number of equations are produced, $\frac{l}{2}$ for each lower and higher boundary, respectively. At the collocation points, equation (23) is used to produce the remaining $N - l + 1$ equations. To proceed this, the collocation points are produced using the following expression:

$$\zeta_i = A + \frac{(B - A)i}{N - (l - 2)}, \quad i = 1, 2, \ldots, N - (l - 1) \text{ in } \zeta \in [A, B]. \tag{24}$$

By using these collocation points, equation (23) can be approximated as follows:

$$\sum_{j=0}^{N} a_j(p_j^*(\zeta_i)Q(\zeta_i)) = M(\zeta_i), \tag{25}$$

for $i = 1, 2, \ldots, N - (l - 1)$ and a_j, $j = 0, 1, \ldots, N$.

3.1 Application of LPCM

Consider the following equations:

$$\frac{f'''}{A_1A_2} - (f')^2 + ff'' + \gamma_1\left(\frac{\eta}{2}f'' - f'\right) - \frac{\lambda}{A_1A_2}f' = 0, \quad (26)$$

$$\frac{k_{\text{thnf}}}{k_{\text{f}}}\frac{\theta''}{\text{Pr}} + A_3\left(\theta' f - \gamma_1\frac{\eta}{2}\theta'\right) + \text{Hs}\,\theta = 0, \quad (27)$$

$$\frac{\chi''}{\text{Sc}} + \chi' f - \gamma_1\frac{\eta}{2}\chi' - \frac{\tau_1}{A_1A_2}(\theta'\chi' + \chi\theta'') = 0, \quad (28)$$

with the particular values of parameters $\gamma_1 = 0.001$, $\text{Pr} = 6.2$, $\tau_1 = 0.1$, $\text{Hs} = 0.5$, $\text{Sc} = 0.8$, and $\lambda = 0.5$. The following describes the approximate solution to the aforementioned equations:

$$f(\eta) = \sum_{j=0}^{4} M_j L_j, \quad (29)$$

$$\theta(\eta) = \sum_{j=0}^{4} N_j L_j, \quad (30)$$

$$\chi(\eta) = \sum_{j=0}^{4} P_j L_j, \quad (31)$$

where M_j, N_j, P_j are the coefficients of Laguerre polynomials. The appropriate solution at each of the boundary points should be determined simultaneously approximating the solution. Consequently, the subsequent computations have been established.

$$M_0 + M_1 + M_2 + M_3 + M_4 = 0\,, \quad (32)$$

$$-M_1 - 2M_2 - 3M_3 - 4M_4 = 1, \quad (33)$$

$$-M_1 - M_2 - \frac{M_3}{2} + \frac{M_4}{6} = 0, \quad (34)$$

$$N_0 + N_1 + N_2 + N_3 + N_4 = 1, \quad (35)$$

$$N_0 - \frac{N_2}{2} - \frac{2N_3}{3} - \frac{5N_4}{8} = 0, \quad (36)$$

$$P_0 + P_1 + P_2 + P_3 + P_4 = 1, \quad (37)$$

$$P_0 - \frac{P_2}{2} - \frac{2P_3}{3} - \frac{5P_4}{8} = 0. \quad (38)$$

Table 1: Thermophysical characteristics of nanoparticles and the base fluid [52,53]

Material	C_p (J kg^{-1} K^{-1})	ρ (kgm^{-3})	k (kg ms^{-3} K^{-1})
(H_2O) Water	4,179	997.1	0.613
(Al_2O_3) Aluminum oxide	765	3,970	40
(Ag) Silver	235	10,500	429
(Cu) Copper	385	8,933	401

The remaining terms can be obtained *via* equation (23) estimated at the collocation points specified in equation (24). The corresponding equations obtained at the collocation points are given in Appendix. By solving equations (32)–(38) and equations provided in appendix, the required number of polynomial coefficients is obtained, which is given as follows:

$$\begin{aligned} &M_0 = -0.31751407,\ \ M_1 = 2.6715225,\\ &M_2 = -4.5949016,\ \ M_3 = 3.4452919,\ \ M_4 = -1.2043988,\\ &N_0 = -23.129720,\ \ N_1 = 109.64281,\ \ N_2 = -192.14243,\\ &N_3 = 151.15576,\ \ N_4 = -44.526419,\\ &P_0 = -1.9170741,\ \ P_1 = 10.100317,\ \ P_2 = -16.300250,\\ &P_3 = 12.838114,\ \ P_4 = -3.7211070. \end{aligned} \quad (39)$$

By substituting the given values in equations (29)–(31), the solution to equations (26)–(28) is achieved, and it has been represented as follows:

$$f(\eta) = -7 \times 10^{-8} + \eta - 0.74271\eta^2 + 0.22872\eta^3 - 0.050183\eta^4, \quad (40)$$

$$\theta(\eta) = 1 - 0.71955\eta - 2.9168\eta^2 + 4.4917\eta^3 - 1.8553\eta^4, \quad (41)$$

$$\chi(\eta) = 1 - 1.1297\eta - 0.056275\eta^2 + 0.34105\eta^3 - 0.15505\eta^4. \quad (42)$$

4 Results and discussion

This section presents the interpretation of arising physical characteristics on three distinct profiles. Temperature and concentration profiles for the NH and CWT examples were shown along with the physical explanation. The approximate

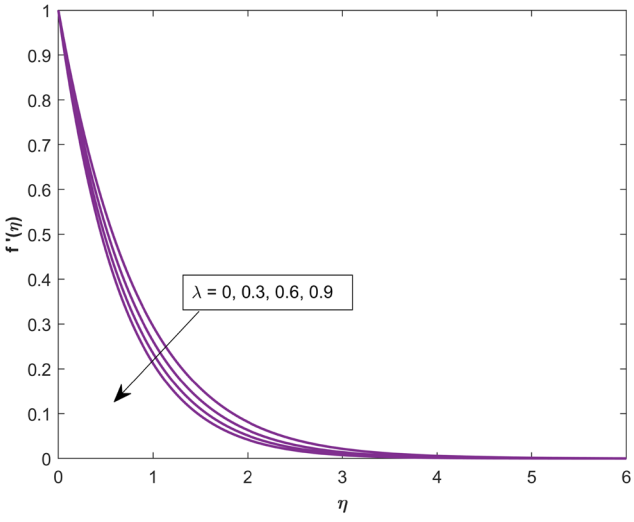

Figure 2: Impact of λ on f'.

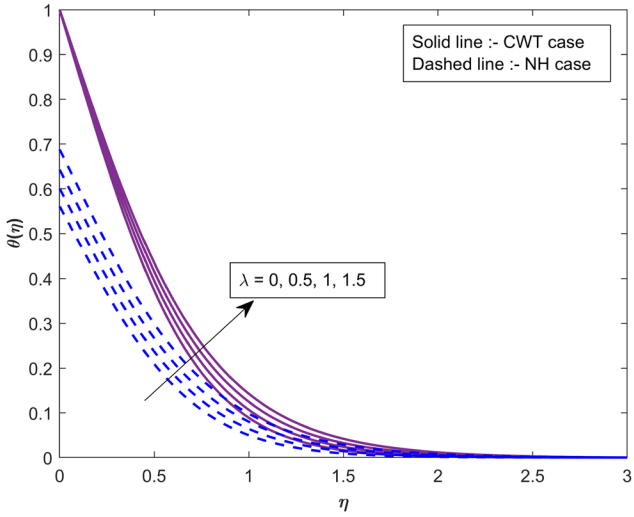

Figure 3: Impact of λ on θ.

LPCM is shown for velocity, temperature, and concentration profiles. In addition, Table 1 displays the thermophysical characteristic values of nanoparticles and the base liquid.

Figure 2 exhibits the role of the porosity parameter λ on velocity. It is obtained that an increase in λ yields a reduction in fluid movement. This is because a greater amount of porous media will suffer drag force and impede fluid travel, which will lower the fluid's velocity. Figure 3 shows the role of λ on the temperature profile $\theta(\eta)$ for NH and CWT cases. Advance in λ will enhance the system's temperature dispersal. This is due to the thermal boundary layer has grown due to an improvement in the porosity factor. The illustration makes it evident that there is less thermal dispersion in the NH case than in the CWT scenario.

Figure 4 demonstrates the significance of Hs on $\theta(\eta)$ for CWT and NH cases. The heat circulation inside the system will intensify as Hs values rise. The heat sink will physically act as an exchanger, bringing heat from the outside into the nanofluid. As a significance, with heat sink, the thermal circulation is minimum, and in the case of the heat source, the surface produces the temperature. In this case, the heat source shows improved thermal dispersion than the heat sink. In comparison to the CWT scenario, the NH case exhibits a greater amount of heat dispersion. The influence of τ_1 on $\chi(\eta)$ is exposed in Figure 5. The upsurge in τ_1 values will decline $\chi(\eta)$. This is because an elevation in the temperature gradient causes particle mobility. Consequently, as τ_1 values rise, the concentration decreases. In

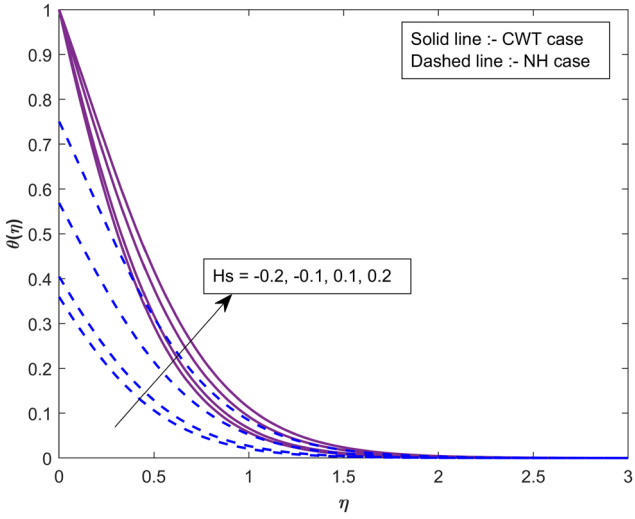

Figure 4: Impact of Hs on θ.

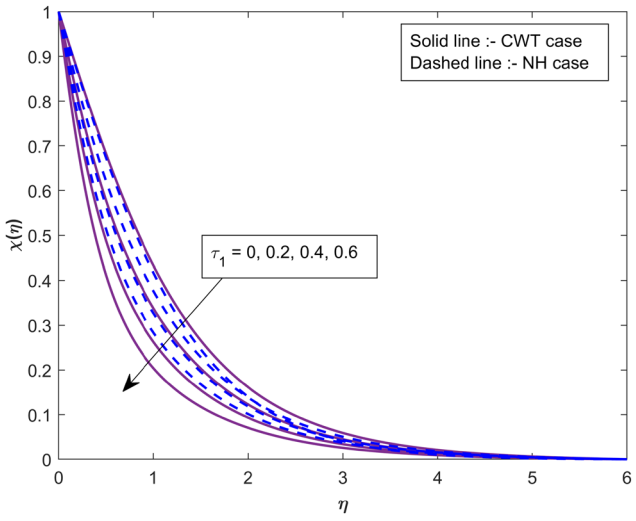

Figure 5: Impact of τ_1 on χ.

comparison to CWT cases, NH cases have greater concentration.

Figure 6 displays the impact of the porosity parameter and ϕ_3 on skin friction. Upsurge in ϕ_3 reduces the surface drag force. This causes due to increase in solid volume percentage raise the momentum boundary layer's thickness and increasing the porosity parameter progressively alter the liquid's flow, which decreases the surface drag force. Figure 7 illustrates the consequence of Nu_x on Hs for numerous values of ϕ_3. As the values of ϕ_3 rise, the rate of heat transmission increases. Furthermore, the figure illustrates how the rate of thermal dispersion falls when the Hs values increase from −0.1 to 0.1. Specifically, in the CWT scenario, the thermal distribution rate decreases from sink to source, but in the NH situation, the opposite tendency is seen. Also, improvement of ϕ_3 rises the thermal boundary layer leading to enhancement in Nu_x with the upsurge of Hs from sink to source. Compared to the NH instance, the CWT case has a higher heat transmission rate. Figure 8 depicts the difference of Sh_x on τ_1 for numerous values of ϕ_3. The mass transport rate drops with the increase in values of ϕ_3 and τ_1. The reason for this is that temperature differences in τ_1 cause molecules to move more quickly, which lowers the mass transport rate. The addition of ϕ_3 will reduce the mass transport rate due to vary in τ_1 values. Further, Table 2 is presented to exhibit the results of numerical solutions achieved using LPCM, which are compared against RKF-45 results. The compared outcomes of $-\mathrm{Cf}_x$, Nu_x, and Sh_x reveal appealing convergence among them. Table 3 is the validation table for the current work

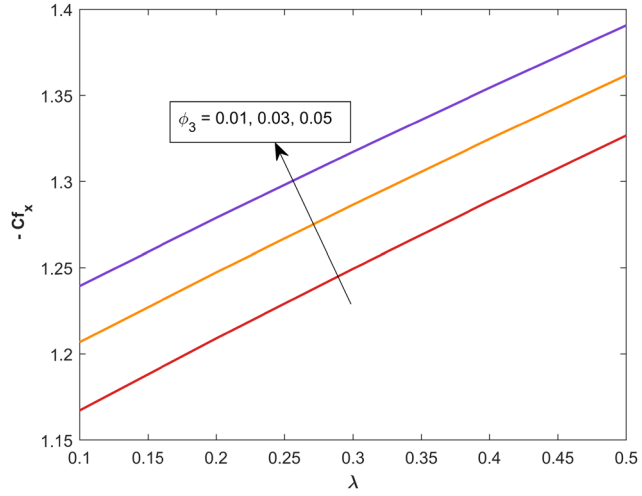

Figure 6: Impact of λ and ϕ_3 on Cf_x.

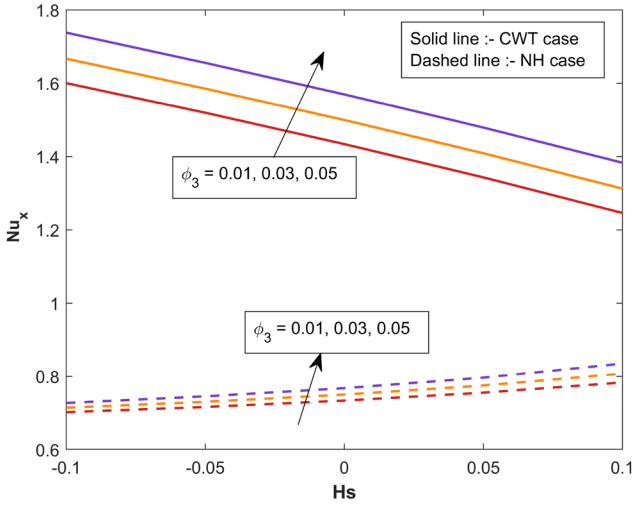

Figure 7: Impact of Hs and ϕ_3 on Nu_x.

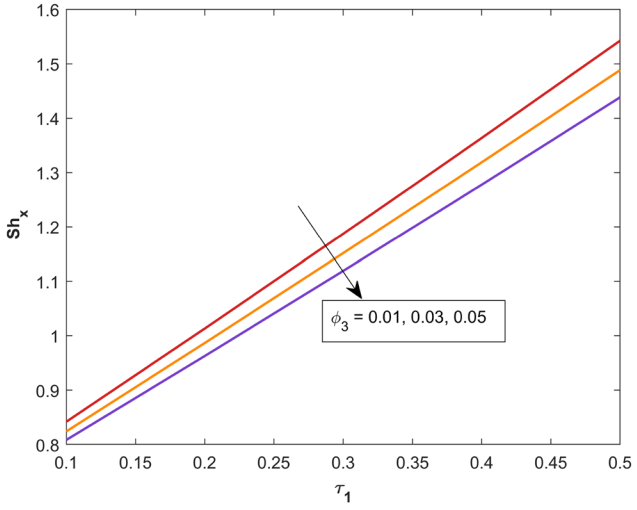

Figure 8: Impact of τ_1 and ϕ_3 on Sh_x.

with the existing literature by limiting the values $A_1 = A_2 = \gamma_1 = 0$. The outcomes will best match each other.

Table 4 shows the computational values of Cf_x%, Nu_x% (CWT and NH cases) [52], and Sh_x% for $\gamma_1 = 0.1$, $\phi_1 = \phi_2 = \phi_3 = 0.01$ for ternary nanofluid and $\phi_3 = 0.01$ for nanofluid. It has been determined that the rate of thermal distribution is enhanced by approximately 2.73% in the CWT case, 4.73% in the NH case, and 2.99% in the rate of mass transfer when transitioning from a ternary hybrid nanofluid to a (normal) nanofluid, for different values of parameters. Hence, the ternary nanofluid shows significant improvement than nanofluid in engineering factors.

Table 2: Comparative assessment of LPCM results with RKF-45 outcomes

Physical quantities	RKF-45	LPCM	Error
$-Cf_x$	1.510949	1.48542	0.025529
Nu_x	0.8196231	0.71955	0.1000731
Sh_x	1.113947	1.1297	0.015753

Table 3: Comparison of the $f''(0)$ values for published work and present study for $A_1 = A_2 = \gamma_1 = 0$

Parameter λ	Kameswaran *et al.* [51]		Present work
	SRM	Analytical	
1	1.41421356	1.41421356	1.14142164
2	1.73205081	1.73205081	1.73205085
5	2.44948974	2.44948974	2.44948974
10	3.31662479	3.31662479	3.31662479

Table 4: Computational values of $Cf_x\%$, $Nu_x\%$ (CWT and NH cases), and $Sh_x\%$ for $\gamma_1 = 0.1$, $\phi_1 = \phi_2 = \phi_3 = 0.01$ for ternary nanofluid and $\phi_3 = 0.01$ for nanofluid case

λ	Hs	τ_1	$Cf_x\%$	$Nu_x\%$		$Sh_x\%$
				CWT	NH	
0.1	0.1	0.1	3.281405	—	—	—
0.2	0.1	0.1	3.070633	—	—	—
0.3	0.1	0.1	2.883793	—	—	—
0.4	0.1	0.1	2.725145	—	—	—
0.5	0.1	0.1	2.570317	—	—	—
0.1	−0.1	0.1	—	4.253149	1.708205	—
0.1	−0.05	0.1	—	4.434492	1.930449	—
0.1	0	0.1	—	4.668223	2.173044	—
0.1	0.05	0.1	—	4.968768	2.541608	—
0.1	0.1	0.1	—	5.371838	3.033304	—
0.1	0.1	0.1	—	—	—	2.15967
0.1	0.1	0.2	—	—	—	2.696128
0.1	0.1	0.3	—	—	—	3.091351
0.1	0.1	0.4	—	—	—	3.388931
0.1	0.1	0.5	—	—	—	3.634531

5 Conclusions

This study investigates the effects of HSS, TPD, and porous media on the time-dependent T-HNF stream over a stretchable surface under NH and CWT conditions. The researched model's governing equations are converted into ODEs with the use of appropriate similarity transformations. The LPCM is employed to solve the resulting dimensionless equations. The key elements identified in the current study are as follows:

- As the porosity parameter increases, the velocity profile decreases.
- The thermal profile will intensify in the occurrence of permeable media and a HSS parameter.
- With an improvement in the thermophoretic parameter, the concentration falls.
- The surface drag force is high in the presence of porosity factor and solid volume fraction.
- Compared to the NH scenario, the CWT case has a higher rate of heat dispersion.
- By comparing the LPCM outcomes with the RKF-45 findings, the suggested approach's efficiency and accuracy were confirmed. Also, the computational approach proved trustworthy for the under considered polynomials and collocation points.
- The solution resulting from LPCM highlights the effectiveness of this approach in dealing with the developed nonlinear problem. Furthermore, it has been demonstrated to obtain appropriate approximations for this problem by employing a minimal number of Laguerre polynomials expansion terms.

The present study is limited to examine the heat and mass transfer of HSS, TPD, and porous media impacts on the time-dependent T-HNF stream over a stretchable surface with NH and CWT conditions. The present work can be extended to examine various nanoparticle combinations, different fluid models, and aggregation impacts with different physical conditions.

Acknowledgments: The authors acknowledge the funding by the Universiti Kebangsaan Malaysia project number "DIP-2023-005." Also, the authors extend their appreciation to the Researchers Supporting Project number (RSPD2024R999), King Saud University, Riyadh, Saudi Arabia. In addition, this research was funded by the Scientific Deanship of Zarqa University, Jordan.

Funding information: This work has been funded by the Universiti Kebangsaan Malaysia project number "DIP-2023-005." Also, the authors extend their appreciation to the Researchers Supporting Project number (RSPD2024R999), King Saud University, Riyadh, Saudi Arabia. In addition, this research was funded by the Scientific Deanship of Zarqa University, Jordan.

Author contributions: K.K and J.K.M: conceptualization, methodology, software, formal analysis, validation, and writing – original draft. R.S and R.S.V.K: writing – original draft, data curation, investigation, visualization, and validation. A.I: conceptualization, writing – original draft, writing – review and editing, supervision, and resources. U.K: validation, software, investigation, writing – review and editing, formal analysis, project administration, and funding acquisition. Md-I.H.S; A.Q: writing – review and editing, writing – original draft, software, data curation, validation, and resources. All authors have accepted responsibility for the entire content of this manuscript and approved its submission.

Conflict of interest: The authors state no conflict of interest.

Data availability statement: The datasets generated and/or analyzed during the current study are available from the corresponding author on reasonable request.

References

[1] Albalawi KS, Karthik K, Madhu J, Bin-Asfour M, Alkahtani BST, Alazman I, et al. Nanoparticle aggregation kinematics and nanofluid flow in convectively heated outer stationary and inner stretched coaxial cylinders: Influenced by linear, nonlinear, and

quadratic thermal radiation. Mod Phys Lett B. 2024;2450361. doi: 10.1142/S0217984924503615.
[2] Kumar TK, Remidi S, Madhu J, Kumar RN, Punith Gowda RJ, Muhammad T, et al. The magnetic dipole-induced ternary-hybrid nanofluid flow behavior along a vertical and horizontal wall under free, mixed, and forced convection. Numer Heat Transfer, Part A: Appl. 2023;1–18. doi: 10.1080/10407782.2023.2296129.
[3] Vinutha K, Sajjan K, Madhukesh JK, Ramesh GK. Optimization of RSM and sensitivity analysis in MHD ternary nanofluid flow between parallel plates with quadratic radiation and activation energy. J Therm Anal Calorim. 2024;149:1595–616. doi: 10.1007/s10973-023-12782-1.
[4] Salawu SO, Akinola EI, Shamshuddin MD. Entropy generation and current density of tangent hyperbolic Cu-C2H6O2 and ZrO2-Cu/C2H6O2 hybridized electromagnetic nanofluid: A thermal power application. South Afr J Chem Eng. 2023;46:1–11. doi: 10.1016/j.sajce.2023.07.003.
[5] Oke AS, Prasannakumara BC, Mutuku WN, Gowda RJP, Juma BA, Kumar RN, et al. Exploration of the effects of Coriolis force and thermal radiation on water-based hybrid nanofluid flow over an exponentially stretching plate. Sci Rep. 2022;12:21733. doi: 10.1038/s41598-022-21799-9.
[6] Madhu J, Vinutha K, Kumar RN, Punith Gowda RJ, Prasannakumara BC, Alqahtani AS, et al. Impact of solid–liquid interfacial layer in the nanofluid flow between stretching stationary disk and a rotating cone. Tribol Int. 2024;192:109187. doi: 10.1016/j.triboint.2023.109187.
[7] Wang F, Iqbal Z, Zhang J, Abdelmohimen MAH, Almaliki AH, Galal AM. Bidirectional stretching features on the flow and heat transport of Burgers nanofluid subject to modified heat and mass fluxes. Waves Random Complex Media. 2022;1–18. doi: 10.1080/17455030.2022.2055203.
[8] Khan SA, Hayat T, Alsaedi A. Thermal conductivity performance for ternary hybrid nanomaterial subject to entropy generation. Energy Rep. 2022;8:9997–10005. doi: 10.1016/j.egyr.2022.07.149.
[9] Karthik K, JK M, Kiran S, KV N, Prasannakumara BC, Fehmi G. Impacts of thermophoretic deposition and thermal radiation on heat and mass transfer analysis of ternary nanofluid flow across a wedge. Int J Model Simul. 2024;1–13. doi: 10.1080/02286203.2023.2298234.
[10] Saadeh R, Al-Smadi M, Gumah G, Khalil H, Khan RA. Numerical investigation for solving two-point fuzzy boundary value problems by reproducing kernel approach. Appl Math Inf Sci. 2016;10:2117–29. doi: 10.18576/amis/100615.
[11] Marin S, Mihail Vlasceanu G, Elena Tiplea R, Raluca Bucur I, Lemnaru M, Minodora Marin M, et al. Applications and Toxicity of Silver Nanoparticles: A Recent Review. Curr Top Med Chem. 2015;15:1596–604.
[12] Beyene HD, Werkneh AA, Bezabh HK, Ambaye TG. Synthesis paradigm and applications of silver nanoparticles (AgNPs), a review. Sustain Mater Technol. 2017;13:18–23. doi: 10.1016/j.susmat.2017.08.001.
[13] Abou El-Nour KMM, Eftaiha A, Al-Warthan A, Ammar RAA. Synthesis and applications of silver nanoparticles. Arab J Chem. 2010;3:135–40. doi: 10.1016/j.arabjc.2010.04.008.
[14] Din MI, Rehan R. Synthesis, characterization, and applications of copper nanoparticles. Anal Lett. 2017;50:50–62. doi: 10.1080/00032719.2016.1172081.
[15] Crisan MC, Teodora M, Lucian M. Copper nanoparticles: synthesis and characterization, physiology, toxicity and antimicrobial applications. Appl Sci. 2022;12:141. doi: 10.3390/app12010141.
[16] Kumar JRN, Almalki ASA, Prasanna BM, Prasad P, Hebbar N, Alsubaie A. Polyethyleneimine–chromium oxide nanocomposite sensor with patterned copper clad as a substrate for CO_2 detection. J Electron Mater. 2022;51:6416–30. doi: 10.1007/s11664-022-09879-y.
[17] Ziva AZ, Suryana YK, Kurniadianti YS, Nandiyanto ABD, Kurniawan T. Recent progress on the production of aluminum oxide (Al2O3) nanoparticles: a review. Mech Eng Soc Ind. 2021;1:54–77. doi: 10.31603/mesi.5493.
[18] Omodele EAA, Adewale AG, Mikaila MM, Joshua IO. A mini-review on the application of alumina nanoparticles for water treatment; 2019.
[19] Pourmadadi M, Farokh A, Rahmani E, Shamsabadipour A, Eshaghi MM, Rahdar A, et al. Porous alumina as potential nanostructures for drug delivery applications, synthesis and characteristics. J Drug Delivery Sci Technol. 2022;77:103877. doi: 10.1016/j.jddst.2022.103877.
[20] Mahesh R, Vora K, Hanumanthaiah M, Shroff A, Kulkarni P, Makuteswaran S, et al. Removal of pollutants from wastewater using alumina based nanomaterials: A review. Korean J Chem Eng. 2023;40:2035–45. doi: 10.1007/s11814-023-1419-x.
[21] Alhadhrami A, Prasanna BM, KC RP, Sarada K, Alzahrani HA. Heat and mass transfer analysis in chemically reacting flow of non-newtonian liquid with local thermal non-equilibrium conditions: a comparative study. Energies. 2021;14:5019. doi: 10.3390/en14165019.
[22] Shamshuddin MD, Salawu SO, Asogwa KK, P, Srinivasa Rao. Thermal exploration of convective transportation of ethylene glycol based magnetized nanofluid flow in porous cylindrical annulus utilizing MOS2 and Fe3O4 nanoparticles with inconstant viscosity. J Magn Magn Mater. 2023;573:170663. doi: 10.1016/j.jmmm.2023.170663.
[23] Wang F, Awais M, Parveen R, Alam MK, Rehman S, deif AMH, et al. Melting rheology of three-dimensional Maxwell nanofluid (graphene-engine-oil) flow with slip condition past a stretching surface through Darcy-Forchheimer medium. Results Phys. 2023;51:106647. doi: 10.1016/j.rinp.2023.106647.
[24] Alhadhrami A, Vishalakshi CS, Prasanna BM, Sreenivasa BR, Alzahrani HAH, Punith Gowda RJ, et al. Numerical simulation of local thermal non-equilibrium effects on the flow and heat transfer of non-Newtonian Casson fluid in a porous media. Case Stud Therm Eng. 2021;28:101483. doi: 10.1016/j.csite.2021.101483.
[25] Dharmendar Reddy Y, Shankar Goud B, Nisar KS, Alshahrani B, Mahmoud M, Park C. Heat absorption/generation effect on MHD heat transfer fluid flow along a stretching cylinder with a porous medium. Alex Eng J. 2023;64:659–66. doi: 10.1016/j.aej.2022.08.049.
[26] Wang F, Jamshed W, Ibrahim RW, Abdalla NSE, Abd-Elmonem A, Hussain SM. Solar radiative and chemical reactive influences on electromagnetic Maxwell nanofluid flow in Buongiorno model. J Magn Magn Mater. 2023;576:170748. doi: 10.1016/j.jmmm.2023.170748.
[27] Chu Y-M, Nazeer M, Khan MI, Hussain F, Rafi H, Qayyum S, et al. Combined impacts of heat source/sink, radiative heat flux, temperature dependent thermal conductivity on forced convective Rabinowitsch fluid. Int Commun Heat Mass Transf. 2021;120:105011. doi: 10.1016/j.icheatmasstransfer.2020.105011.
[28] Thumma T, Mishra SR, Abbas MA, Bhatti MM, Abdelsalam SI. Three-dimensional nanofluid stirring with non-uniform heat source/sink through an elongated sheet. Appl Math Comput. 2022;421:126927. doi: 10.1016/j.amc.2022.126927.
[29] Saadeh R. Numerical solutions of fractional convection-diffusion equation using finite-difference and finite-volume schemes. J Math Comput Sci. 2021;11:7872–91. doi: 10.28919/10.28919/jmcs/6658.

[30] Ram MS, Spandana K, Shamshuddin MD, Salawu SO. Mixed convective heat and mass transfer in a magnetized micropolar fluid flow toward stagnation point on a porous stretching sheet with heat source/sink and variable species reaction. Int J Model Simul. 2023;43:670–82. doi: 10.1080/02286203.2022.2112008.
[31] Wang F, Ahmed A, Naveed Khan M, Ameer Ahammad N, Alqahtani AM, Eldin SM, et al. Natural convection in nanofluid flow with chemotaxis process over a vertically inclined heated surface. Arab J Chem. 2023;16:104599. doi: 10.1016/j.arabjc.2023.104599.
[32] Bai D, Muhammad N, Shah NA, Ali B, Raju CSK, Wakif A, et al. OpenFOAM simulation of turbulent flow in a complex dam structure. Indian J Phys. 2024;98:3277–86. doi: 10.1007/s12648-024-03085-8.
[33] Bashir S, Ramzan M, Ghazwani HAS, Nisar KS, Saleel CA, Abdelrahman A. Magnetic dipole and thermophoretic particle deposition impact on bioconvective oldroyd-B fluid flow over a stretching surface with Cattaneo–Christov heat flux. Nanomaterials. 2022;12:2181. doi: 10.3390/nano12132181.
[34] Wang Y, Kumar RN, Gouadria S, Helmi MM, Gowda RJP, El-Zahar ER, et al. A three-dimensional flow of an Oldroyd-B liquid with magnetic field and radiation effects: An application of thermophoretic particle deposition. Int Commun Heat Mass Transf. 2022;134:106007. doi: 10.1016/j.icheatmasstransfer.2022.106007.
[35] Yasir M, Khan M, Malik ZU. Analysis of thermophoretic particle deposition with Soret-Dufour in a flow of fluid exhibit relaxation/retardation times effect. Int Commun Heat Mass Transf. 2023;141:106577. doi: 10.1016/j.icheatmasstransfer.2022.106577.
[36] Shamshuddin MD, Agbaje TM, Asogwa KK, Makanda G, Usman. Chebyshev spectral approach to an exponentially space-based heat generating single-phase nanofluid flowing on an elongated sheet with angled magnetic field. Numer Heat Transfer, Part B: Fundam. 2024;85:159–76. doi: 10.1080/10407790.2023.2230355.
[37] Alsaiari AO, Iqbal A, Abdulkhair H, Gzara L, Almatrafi E, Alzahrani HAH, et al. Heat transmission and air flow friction in a solar air heater with a ribbed absorber plate: A computational study. Case Stud Therm Eng. 2022;40:102517. doi: 10.1016/j.csite.2022.102517.
[38] Saadeh R, Abdoon MA, Qazza A, Berir M, Guma FE, Al-kuleab N, et al. Mathematical modeling and stability analysis of the novel fractional model in the Caputo derivative operator: A case study. Heliyon. 2024;10:e26611. doi: 10.1016/j.heliyon.2024.e26611.
[39] Shamshuddin MD, Agbaje TM, Asogwa KK, Ramesh K. Computational investigation for silica-molybdenum disulfide/water-based hybrid nanofluid over an exponential stretching sheet with spectral quasi-linearization method. Numer Heat Transfer, Part B: Fundam. 2023;1–25. doi: 10.1080/10407790.2023.2289503.
[40] Shamshuddin MD, Saeed A, Mishra SR, Katta R, Eid MR. Homotopic simulation of MHD bioconvective flow of water-based hybrid nanofluid over a thermal convective exponential stretching surface. Int J Numer Methods Heat Fluid Flow. 2023;34:31–53. doi: 10.1108/HFF-03-2023-0128.
[41] Madhu J, Saadeh R, Karthik K, Kumar RV, Kumar RN, Gowda RP, et al. Role of catalytic reactions in a flow-induced due to outer stationary and inner stretched coaxial cylinders: An application of Probabilists' Hermite collocation method. Case Stud Therm Eng. 2024;56:104218.
[42] Epstein M, Hauser GM, Henry RE. Thermophoretic deposition of particles in natural convection flow from a vertical plate. J Heat Transf. 1985;107:272–6. doi: 10.1115/1.3247410.
[43] Vinothkumar B, Saadeh R, Poornima T, Qazza A, Sreenivasulu P, Subba Rao A, et al. Two-phase numerical simulation of thermal and solutal transport exploration of a non-Newtonian nanomaterial flow past a stretching surface with chemical reaction. Open Phys. 2024;22(1):20240036.
[44] Salleh MZ, Nazar R, Pop I. Boundary layer flow and heat transfer over a stretching sheet with Newtonian heating. J Taiwan Inst Chem Eng. 2010;41:651–5. doi: 10.1016/j.jtice.2010.01.013.
[45] Talbot L, Cheng RK, Schefer RW, Willis DR. Thermophoresis of particles in a heated boundary layer. J Fluid Mech. 1980;101:737–58. doi: 10.1017/S0022112080001905.
[46] Batchelor GK, Shen C. Thermophoretic deposition of particles in gas flowing over cold surfaces. J Colloid Interface Sci. 1985;107:21–37. doi: 10.1016/0021-9797(85)90145-6.
[47] Sagot B. Thermophoresis for spherical particles. J Aerosol Sci. 2013;65:10–20. doi: 10.1016/j.jaerosci.2013.06.007.
[48] Prodi F, Santachiara G, Di Matteo L, Vedernikov A, Beresnev SA, Chernyak VG. Measurements of thermophoretic velocities of aerosol particles in microgravity conditions in different carrier gases. J Aerosol Sci. 2007;38:645–55. doi: 10.1016/j.jaerosci.2007.04.002.
[49] Sagot B, Antonini G, Buron F. Annular flow configuration with high deposition efficiency for the experimental determination of thermophoretic diffusion coefficients. J Aerosol Sci. 2009;40:1030–49. doi: 10.1016/j.jaerosci.2009.09.009.
[50] Ramesh GK, Madhukesh JK, Das R, Shah NA, Yook S-J. Thermodynamic activity of a ternary nanofluid flow passing through a permeable slipped surface with heat source and sink. Waves Random Complex Media. 2022;1–21. doi: 10.1080/17455030.2022.2053237.
[51] Kameswaran PK, Makukula ZG, Sibanda P, Motsa SS, Murthy PVSN. A new algorithm for internal heat generation in nanofluid flow due to a stretching sheet in a porous medium. Int J Numer Methods Heat Fluid Flow. 2014;24:1020–43. doi: 10.1108/HFF-10-2012-0224.
[52] Madhu J, Madhukesh JK, Sarris I, Prasannakumara BC, Ramesh GK, Shah NA, et al. Influence of quadratic thermal radiation and activation energy impacts over oblique stagnation point hybrid nanofluid flow across a cylinder. Case Stud Therm Eng. 2024;60:104624. doi: 10.1016/j.csite.2024.104624.
[53] Rana P, Bhargava R. Numerical study of heat transfer enhancement in mixed convection flow along a vertical plate with heat source/sink utilizing nanofluids. Commun Nonlinear Sci Numer Simul. 2011;16:4318–34. doi: 10.1016/j.cnsns.2011.03.014.

Appendix

$$
\begin{aligned}
&-2.3889M_2^2 + (-2.6667M_1 - 5.6543M_3 - 5.5746M_4 + M_0 + 0.74795)M_2\\
&-3.7973M_3^2 + (-2.3333M_1 - 8.4170M_4 + 2.6667M_0 + 0.026493)M_3\\
&-5.0250M_4^2 + (-1.2840M_1 + 4.7222M_0 - 2.2904)M_4 - M_1^2 + 0.44887M_1 = 0,
\end{aligned}
\tag{A1}
$$

$$
\begin{aligned}
&-1.8889M_2^2 + (-2.3333M_1 - 3.9012M_3 - 3.1564M_4 + M_0 + 0.59816)M_2\\
&-2.3868M_3^2 + (-1.6667M_1 - 4.6324M_4 + 2.3333M_0 - 0.34790)M_3\\
&-2.5630M_4^2 + (-0.49383M_1 + 3.5556M_0 - 2.6102)M_4 - M_1^2 + 0.44887M_1 = 0,
\end{aligned}
\tag{A2}
$$

$$
\begin{aligned}
&(0.37834 - M_0 - 0.75000M_1 - 0.53125M_2 - 0.34115M_3 - 0.17725M_4)N_1\\
&+(0.37703 - 1.7500M_0 - 1.3125M_1 - 0.92969M_2 - 0.59701M_3 - 0.31018M_4)N_2\\
&+(0.47182 - 2.2812M_0 - 1.7109M_1 - 1.2119M_2 - 0.77824M_3 - 0.40434M_4)N_3\\
&+(0.63766 - 2.6224M_0 - 1.9668M_1 - 1.3931M_2 - 0.89462M_3 - 0.46481M_4)N_4\\
&+0.50429N_0 = 0,
\end{aligned}
\tag{A3}
$$

$$
\begin{aligned}
&(0.25239 - M_0 - 0.50000M_1 - 0.12500M_2 + 0.14583M_3 + 0.33073M_4)N_1\\
&+(0.17232 - 1.5000M_0 - 0.75000M_1 - 0.18750M_2 + 0.21875M_3 + 0.49609M_4)N_2\\
&+(0.19914 - 1.6250M_0 - 0.81250M_1 - 0.20312M_2 + 0.23698M_3 + 0.53743M_4)N_3\\
&+(0.28284 - 1.4792M_0 - 0.73958M_1 - 0.18490M_2 + 0.21571M_3 + 0.48920M_4)N_4\\
&+0.50429N_0 = 0,
\end{aligned}
\tag{A4}
$$

$$
\begin{aligned}
&(0.12645 - M_0 - 0.25000M_1 + 0.21875M_2 + 0.47656M_3 + 0.58057M_4)N_1\\
&+(-0.00093430 - 1.2500M_0 - 0.31250M_1 + 0.27344M_2 + 0.59570M_3 + 0.72571M_4)N_2\\
&+(0.0051093 - 1.0312M_0 - 0.25781M_1 + 0.22559M_2 + 0.49146M_3 + 0.59871M_4)N_3\\
&+(0.064796 - 0.55469M_0 - 0.13867M_1 + 0.12134M_2 + 0.26434M_3 + 0.32203M_4)N_4\\
&+0.50429N_0 = 0,
\end{aligned}
\tag{A5}
$$

$$
\begin{aligned}
&\begin{pmatrix}-M_0 - 0.75000M_1 - 0.53125M_2 - 0.34115M_3 - 0.17725M_4 - 0.1N_1\\ -0.25000N_2 - 0.43438N_3 - 0.63958N_4 + 0.00012500\end{pmatrix}P_1\\
&+\begin{pmatrix}-1.7500M_0 - 1.3125M_1 - 0.92969M_2 - 0.59701M_3\\ -0.31018M_4 - 0.17500N_1 - 0.35938N_2 - 0.54531N_3 - 0.72620N_4 + 1.2502\end{pmatrix}P_2\\
&+\begin{pmatrix}-2.2812M_0 - 1.7109M_1 - 1.2119M_2 - 0.77824M_3\\ -0.40434M_4 - 0.22812N_1 - 0.43333N_2 - 0.61423N_3 - 0.76987N_4 + 3.4378\end{pmatrix}P_3\\
&+\begin{pmatrix}-2.6224M_0 - 1.9668M_1 - 1.3931M_2 - 0.89462M_3\\ -0.46481M_4 - 0.26224N_1 - 0.47664N_2 - 0.64698N_3 - 0.77687N_4 + 6.2894\end{pmatrix}P_4\\
&-0.1P_0N_2 - 0.27500P_0N_3 - 0.50312P_0N_4 = 0,
\end{aligned}
\tag{A6}
$$

$$
\begin{aligned}
&\begin{pmatrix}-M_0 - 0.50000M_1 - 0.12500M_2 + 0.14583M_3 + 0.33073M_4\\ -0.1N_1 - 0.20000N_2 - 0.28750N_3 - 0.35417N_4 + 0.00025000\end{pmatrix}P_1\\
&+\begin{pmatrix}-1.5000M_0 - 0.75000M_1 - 0.18750M_2 + 0.21875M_3 + 0.49609M_4\\ -0.15000N_1 - 0.23750N_2 - 0.27500N_3 - 0.27344N_4 + 1.2504\end{pmatrix}P_2\\
&+\begin{pmatrix}-1.6250M_0 - 0.81250M_1 - 0.20312M_2 + 0.23698M_3 + 0.53743M_4\\ -0.16250N_1 - 0.22917N_2 - 0.22760N_3 - 0.18021N_4 + 3.1254\end{pmatrix}P_3\\
&+\begin{pmatrix}-1.4792M_0 - 0.73958M_1 - 0.18490M_2 + 0.21571M_3 + 0.48920M_4\\ -0.14792N_1 - 0.18880N_2 - 0.15768N_3 - 0.082368N_4 + 5.1566\end{pmatrix}P_4\\
&-0.1P_0N_2 - 0.25000P_0N_3 - 0.41250P_0N_4 = 0,
\end{aligned}
\tag{A7}
$$

$$
\begin{aligned}
&\begin{pmatrix} -M_0 - 0.25000M_1 + 0.21875M_2 + 0.47656M_3 + 0.58057M_4 - 0.1N_1 \\ -0.15000N_2 - 0.15938N_3 - 0.13750N_4 + 0.00037500 \end{pmatrix} P_1 \\
&+\begin{pmatrix} -1.2500M_0 - 0.31250M_1 + 0.27344M_2 + 0.59570M_3 + 0.72571M_4 \\ -0.12500N_1 - 0.13438N_2 - 0.079688N_3 + 0.0024414N_4 + 1.2505 \end{pmatrix} P_2 \\
&+\begin{pmatrix} -1.0312M_0 - 0.25781M_1 + 0.22559M_2 + 0.49146M_3 + 0.59871M_4 \\ -0.10312N_1 - 0.081250N_2 + 0.00087891N_3 + 0.099170N_4 + 2.8129 \end{pmatrix} P_3 \\
&+\begin{pmatrix} -0.55469M_0 - 0.13867M_1 + 0.12134M_2 + 0.26434M_3 + 0.32203M_4 \\ -0.055469N_1 - 0.011279N_2 + 0.073425N_3 + 0.15973N_4 + 4.1018 \end{pmatrix} P_4 \\
&-0.1P_0N_2 - 0.22500P_0N_3 - 0.32812P_0N_4 = 0.
\end{aligned}
\tag{A8}
$$